5-2023

Understanding the Effect of Nanointerfaces on Nanostructure and Mechanical Properties of Semicrystalline Polymers Using Coarse-Grained Molecular Dynamic Simulations

Nayoung Kim

DEVELOPMENT OF 3D OVARIAN CANCER SPHEROIDS *IN VITRO* AND INVESTIGATION OF THEIR PHYSIOLOGICAL RELEVANCE AS MODELS OF INHERENT CHEMORESISTANCE

Amanda Murray

Advisor: Dr. Angela Alexander-Bryant

Mentor: Kharimat Lora Alatise

Departmental Honors in Bioengineering

Clemson University

May 2023

ABSTRACT

Ovarian cancer is the sixth leading cause of death among women worldwide, with an average 5-year survival rate of less than 48%. Current clinical treatment methods for this disease are often deemed ineffective because of the innate chemoresistance of tumors due to their microenvironment and architecture. Accurately mimicking chemoresistance with traditional 2D cultures is difficult; therefore, recent years have seen an increase in 3D culturing methods that create cellular spheroids. These spheroids can serve as models of *in vivo* tumor characteristics due to their hypoxic core, acidic microenvironment, and increased cell-to-cell interactions. This research aims to (1) refine a 3D culture protocol that allows for the consistent formation of ovarian cancer spheroids, and (2) evaluate the spheroids for their physical and molecular properties as it relates to chemoresistance in ovarian cancer.

Both ES-2 and OVCAR-3 ovarian cancer cell lines formed aggregates of 500 μm within 24 hours of seeding, yet the ES-2 spheroids were much more compact than the OVCAR-3 aggregates. 3D ES-2 cultures showed significantly increased chemoresistance to treatment with chemotherapeutic paclitaxel in comparison to 2D ES-2 cultures. Histochemical staining of ES-2 spheroids showed tight cellular congregation along the outer rim of the spheroid and sparse cellular distribution near the core, meaning that outer cells are proliferating whereas core cells are necrotic. From this, we concluded that our spheroids display a structure similar to those noted as recapitulating *in vivo* tumors in previous literature. Lastly, western blotting revealed that changes in protein expression began to occur at four days of spheroid growth.

Our results demonstrate morphological differences in tumor spheroids of two different ovarian cancer cell lines. Additionally, we've found that cells grown in 3D display increased chemoresistance in comparison to 2D-cultured cells, confirming the spheroids' ability to provide translatable *in vitro* results compared to *in vivo* tumor characteristics. Lastly, the spheroids displayed concentric cellular zones that indicate tumor-like spheroid formation according to previous literature, as well as differential expression of oncogenic proteins compared to traditional 2D cultures.

TABLE OF CONTENTS

LIST OF FIGURES

Schemes

Figures

BACKGROUND AND INTRODUCTION

Ovarian cancer is the most lethal gynecological malignancy in the United States, and in 2023, it is estimated that almost 20,000 women in the United States alone will receive a new diagnosis and over 13,000 women will die from the disease.[1,2] Eighty percent of ovarian cancer patients are diagnosed with a late-stage form of the disease (stage III or later), and the 5-year survival rate of this patient population is only 30.3%.[3,4] At late stages, the disease has metastasized and spread from the original, localized tumor, forming exceedingly small tumors that survive within abdominal ascites. Once this occurs, the disease is difficult to treat with tumor debulking surgery because these metastases are difficult to capture in totality. While large, localized tumors are capable of full removal, and the patient will likely still undergo intraperitoneal chemotherapy with a platinum- or taxane-based drug regimen to treat the remaining cancer.[6]

Despite initial success with these treatments, ovarian cancer cells often develop a resistance to the drug's therapeutic effects that hinder their efficacy and allow for disease progression.[7] This is a phenomenon known as chemoresistance, and it can be classified as acquired or inherent. Acquired chemoresistance occurs through mutations in the cancerous genome which allows the cell to evade the apoptotic effects of chemotherapeutics through various methods, such as increasing drug efflux proteins or overexpressing oncogenes.[8,9] This type of chemoresistance is commonly referred to as multidrug resistance, and it occurs after repeated treatments with chemotherapeutics.[10] Inherent chemoresistance is a challenge faced in almost all chemotherapeutic ventures as it derives from the three-dimensional architecture of a tumor. As tumors grow, they develop concentric layers of cells that have varying access to oxygen due to the limited

diffusion of oxygen and nutrients from blood vessels. There is also a drug diffusion limit with blood vessels, so if a tumor becomes too large, it is inherently chemoresistant because some of its inner cells will not be affected by a chemotherapeutic drug in the bloodstream.[11] Additionally, tumors contain cells that become quiescent to survive the lower end of the oxygen and nutrient gradients that penetrate tumors.[50] These cells are slow-dividing due to their suspension in the G0 phase of mitosis, however most chemotherapies target actively dividing cells, rendering them ineffective against this quiescent population.[51,52]

Overall, the inefficacies of current treatment methods present an urgent need for new avenues for fighting ovarian cancer. The testing of new treatment modalities is commonly conducted on two-dimensional, monolayer cell cultures, and then taken for further testing in *in vivo* animal models. This testing regimen often leads to treatments that are effective in *in vitro* cell cultures yet ineffective in animals. While drugs and nanoparticle delivery systems can easily interact with and invade cancer cells that are cultured on a flat surface, they lack this efficacy when faced with the complex structure of a native tumor. To combat this obstacle, recent years have seen an increased interest in three-dimensional cell cultures as more robust in vitro models for cancer therapy testing.

Spheroids have been found to exhibit accurate tumor-like properties compared to monolayer cell cultures, such as a hypoxic core, an acidic microenvironment, and increased cell to cell interactions.[12] More specifically, spheroids with a diameter of 500 microns or greater express these properties due to their development of three concentric cellular zones: a necrotic core, a quiescent middle layer, and a proliferating outer layer.[13] Furthermore, spheroids are particularly relevant in ovarian cancer research because they

are very similar to the small ovarian cancer tumors that develop within patient ascites that make ovarian cancer treatment so multifaceted and difficult.[14] As previously mentioned, these tumors prevent ovarian cancer treatments from penetrating past the outermost layers of the tumors, rendering the inner bulk of cells protected from the treatment, and in vitro tumor spheroids replicate their treatment barrier very well.[15,16]

With this in mind, the main goal of this study is to develop an easily reproducible culture protocol suited for the creation of uniform ovarian cancer spheroids of 500 microns or greater in diameter that will allow for more translatable modeling of in vivo outcomes during in vitro experiments for the development of novel anticancer therapeutics. The specific properties that enhance the inherent chemoresistance of the spheroids will also be investigated, including the expression of genes and proteins known to be associated with chemoresistance.

Our proteins of interest include ABCB1, CFLAR, and STAT3, all of which have been investigated as proteins that modulate chemoresistance in ovarian cancer cells.[17,18,19] ATP binding cassette B1 (ABCB1), also called p-glycoprotein, is a drug efflux protein that resides on the surface of cells and transports therapeutic agents out of cells to prevent damage.[18,46] CASP8 and FADD-like apoptosis regulator (CFLAR), also known as cFLIP, blocks the recruitment of Caspase 8 and inhibits Caspases 8 and 10, thus inhibiting natural apoptosis in cancerous cells and allowing them to replicate despite their mutated genomes. Signal Transducer and Activator of Transcription 3 (STAT3) is a cytoplasmic protein that is often upregulated in ovarian cancer, both in clinical specimens and in vitro cultures. It regulates many processes within cancer cells, such as tumor growth, cellular survival, and chemoresistance.[17]

MATERIALS AND METHODS

Materials

OVCAR-3 and ES-2 were obtained from ATCC (Manassas, VA). 96-well flat-bottom plates, 96-well ultra-low attachment (ULA) plates, 100X penicillin-streptomycin, and fetal bovine serum (FBS) were purchased from Corning (Corning, NY). McCoy's 5A medium and RPMI medium 1640 was purchased from Gibco (Waltham, MA). T-75 flasks and ultra-pure dimethyl sulfoxide (DMSO) were purchased from VWR International (Radnor, PA). CellTiter 96® Aqueous One Solution Cell Proliferation Assay Kit (MTS Assay Kit) was purchased from Promega (Madison, WI). Powdered methylcellulose and noble agar were purchased from Sigma-Aldrich (St. Louis, MO). Paclitaxel was purchased from LC Laboratories (Woburn, MA). Tissue Plus OCT Compound was purchased from Scigen Scientific Inc. (Gardena, CA). Rapid Richard-Allen™ hematoxylin and eosin were purchased from Fisher Scientific (Hampton, NH). Diamond White Glass microscope positively charged slides were purchased from Globe Scientific Inc. (Mahwah, NJ). S-Mounting Medium, Acrylic was purchased from Azer Scientific (Morgantown, PA).

2D cell culture

Cells (ES-2 and OVCAR-3) were recovered and cultured within T-75 flasks and maintained at 37 °C and 5% CO_2 in an incubator according to ATCC recommended protocols. When confluent, the cells were tryspinized, suspended, and counted. Cell suspensions were diluted with complete media composed of base medium (McCoy's for ES-2 cells; RPMI for OVCAR-3 cells) with 10% Fetal Bovine Serum (FBS) and 1% penicillin-streptomycin (P/S), with or without 0.5% W/V methylcellulose to desired cell

seeding densities. Cells were then seeded into 96-well flat bottom plates at a well volume of 100 microliters for two dimensional experiments.

3D cell culture

Cells (ES-2 and OVCAR-3) were recovered and cultured within T-75 flasks and maintained at 37°C and 5% CO_2 in an incubator until confluent, then trypsinized, suspended, and counted. Cell suspensions were diluted with complete media to desired cell seeding densities. Cells were then seeded in 96-well ultra-low attachment (ULA) plates at a volume of 100 microliters per well. The ULA plates were immediately centrifuged at 300 G for 3 minutes (Scheme 1A). Media was changed in the spheroids every three days via a 50-50 method in which 50 µL of used media in each well was removed and replaced with 50 µL of fresh complete media via micropipette. Spheroids were imaged each day with a 4X phase microscope lens and then analyzed using ImageJ software to determine spheroid diameter. Additionally, non-adherent cell culture plates were simulated using a flat-bottom 96-well plate with 50 µL of cooled agarose in each well (Scheme 1B). The agarose used was 1.5% weight/volume, formulated with agar powder and complete media. OVCAR-3 cells were seeded in all three-dimensional plates at concentrations of 10,000, 15,000, 20,000, and 25,000 cells per well. ES-2 cells were seeded in all three-dimensional plates at seeding concentrations of 2,500, 5,000, 10,000, and 15,000 cells per well. All cells were seeded into the three-dimensional well plates at a working volume of 100 microliters.

Addition of 0.5% Methylcellulose

Methylcellulose was added to the complete media of both ES-2 and OVCAR-3 spheroids to observe its effect on spheroid compactness based on previous literature14.

The methylcellulose-treated media was synthesized as 0.5% weight/volume, with 150 mg of powdered methylcellulose added to 30 mL of complete media, and then used for cell diluting and seeding.

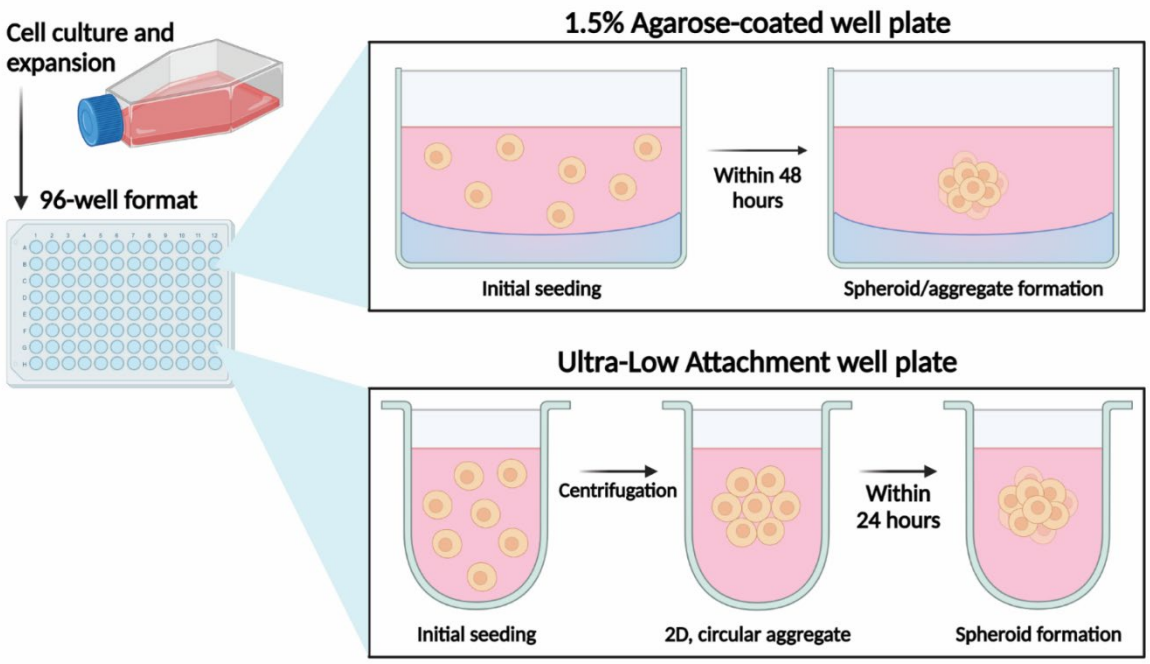

Scheme 1: Rendering of spheroid culture protocol using 1.5% agarose-coated and ultra-low attachment 96-well plates. Pink coloring represents complete cell culture media; yellow circles represent ovarian cancer cells; blue coloring represents agarose coating. Created with BioRender.com.

Paclitaxel treatment

Paclitaxel (PTX) treatments were diluted from an initial stock solution created immediately before each experiment, such that 0.853 milligrams of PTX dissolved in 1 milliliter of DMSO constitutes a stock of 1 millimolar PTX. The 1 mM stock was then diluted with 0.2-micron filtered deionized water (ddH_2O) to the final treatment stock concentrations desired in the micromolar range. Monolayer wells were treated with PTX,

ddH_2O, and transfection media (80% base medium + 20% FBS) to a total well volume of 100 µL after complete aspiration of well contents. Spheroid wells were treated with PTX, ddH2O, and transfection media to a total well volume of 200 µL (100 µL of new solution + 100 µL of previous well contents). Both 2D and 3D cells were seeded at 5,000 cells/well in triplicate for cellular viability assays, and the effect of PTX was assessed after 48 hours of treatment.

Metabolic activity assays

Spheroids were grown for 4 days after seeding then were treated with varying concentrations of PTX. After 48 hours, 2D and 3D wells were treated with 10 and 20 µL of MTS, respectively, and after 3 hours of incubation, plate absorbance was read via spectrophotometer at 490 nm. Before calculating the percent of cellular viability in each well, the average absorbance of each treatment triplicate was normalized with the absorbance of the untreated (0 M PTX) wells.

Histological sectioning and staining

Spheroids were grown for 3 days before fixation for sectioning. Spheroids were removed from their respective wells and transferred to one well of a 24-well plate. The complete media of the spheroids was carefully removed via micro-pipetting without disturbing or damaging the spheroids. Next, a 30% W/V sucrose solution was added with a plastic dropper at a volume large enough to submerse all spheroids, and the well was allowed to sit for one hour. Next, the 30% W/V sucrose solution was carefully removed via micropipette and a 50/50 solution of OCT (Optimal Cutting Temperature) solution and 30% sucrose was made. The spheroids were submerged in this solution and allowed to sit for at least one hour. Lastly, the 50/50 solution was aspirated from the spheroids via

micropipette and replaced with pure OCT gel. The spheroids were then set aside for 24 hours to complete the fixation process. Once fixed, the spheroids were sectioned into 5-micron slices with a Microm HM 550 Cryostat (ThermoFisher Scientific, Waltham, MA) and placed on glass slides for staining with hematoxylin and eosin.

Western Blotting

For 3D analyses, ES-2 cells were seeding at 10,000 cells/well and for 2D analyses, ES-2 cells were seeded at 15,000 cell/well. Cells were kept in standard cell culture conditions for two, three, and four days. For protein isolation, cells were washed with 1X PBS and lysed with radioimmunoprecipitation assay (RIPA) buffer, supplemented with protease inhibitor cocktail (ThermoFisher). Protein concentrations were deterred via bicinchoninic assay (BCA), according to the manufacturer's protocol, and absorbance was read at 562 nanometers. Equal protein concentrations were separated by SDS-PAGE on a Bio-Rad Stain-Free 10% gel, according to manufacturer's protocol, and transferred to a stain-free PVDF membrane via wet transfer system. The PVDF membrane was cut at appropriate molecular weight intervals consistent with protein weight analyzed and blocked for one hour with 5% W/V non-fat dried milk solution in 1X Tris—HCl-buffered saline 0.1% Tween 20 (TBST) at room temperature. Blots were probed at 4 degrees Celsius with a monoclonal anti-ABCB1, anti-CFLAR or anti-STAT3. Membranes were washed five times with 1X TBST and incubated with corresponding goat anti-rabbit or goat anti-mouse secondary antibodies for one hour at room temperature. Five additional washes with 1X TBST were performed, and protein bands were detected with SuperSignal West Pico Plus Chemiluminescent Substrate (ThermoFisher) and imaged using a Bio-Rad ChemiDoc Imaging System.

qPCR

For 3D analyses, ES-2 cells were seeded at 10,000 cells/well as described previously and trypsinized, and for 2D analyses, ES-2 cells were seeded at 70,000 cells/well as described previously and trypsinized. Cells were kept in standard cell culture conditions for two, three, and four days. RNA isolation was completed with a Qiagen Mini-RNeasy Kit (Qiagen, Hilden, Germany), according to manufacturer's protocol. RNA isolate quality and quantity were measured using a Take3 plate (Biotek, Winooksi, VT) with Gen5 analysis software, and isolated RNA was then reverse transcribed with QuantiTect Reverse Transcription kit (Qiagen, Hilden, Germany). Using 200 ng of RNA, real-time qPCR was performed with a QuantStudio 3 qPCR system (Applied Biosystems, Waltham, MA), using Taqman FAST Master Mix (ThermoFisher Scientific) and ABCB1, CFLAR, STAT3, and 18S Taqman probes, according to the manufacturer's protocol.

Flow cytometry

For flow cytometric analyses, 3D ES-2 cells were seeded at 5,000 cells/well as described previously and trypsinized. The single-cell suspension was then resuspended in 1X PBS for 3 minutes and fixed with 0.4% paraformaldehyde for 15 minutes, then resuspended in 1X PBS. Cells were then stained with Annexin V-FITC Apoptosis detection kit (Affymetrix eBioscience, Santa Clara, CA) according to the manufacturer's protocol. Cells were analyzed with an Attune NXT Acoustic flow cytometer (Invitrogen, Carlsbad, CA).

Statistical analyses

This data is presented as mean ± standard error (SEM). Statistical significance was analyzed via multiple t-tests between the 2D and 3D cellular viability at each

treatment concentration of PTX. Analyses were performed at a confidence level of 95%, with probability values of * $p < 0.05$, ** $p < 0.01$, *** $p < 0.005$, and **** $p < 0.001$ considered statistically significant.

RESULTS

Spheroid culture protocols

OVCAR-3 cells: OVCAR-3 cells were seeded in ULA and agarose-coated plates with and without 0.5% MC and imaged over the course of four days (Figure 1). We observed the formation of large aggregates as soon as 48 hours on both culture surfaces, and the aggregates of higher seeding densities (20 and 25 x 10^3 cells/well) formed more compacted structures. However, the OVCAR-3 cells did not form compact, consistent spheroids over time when cultured without MC. To encourage spheroid compaction, MC was added to the complete culture media at a concentration of 0.5% W/V, based on the chemical's success in OVCAR-3 spheroid compaction in previous literature.[14] Our results did not replicate this finding, but rather, OVCAR-3 aggregates loosened and disaggregated when MC was added on both culture surfaces. We again observed loose aggregates of cells with visible voids and of variable sizes rather than tight spheroids of a consistent or slow-growing size. When measured over the course of seven days, the OVCAR-3 aggregates did reach sizes greater than 500 microns in diameter as soon as 24 hours after seeding (Figure 2B), however they exhibited more variable sizes and increased error in comparison to our ES-2 spheroids (Figure 2A).

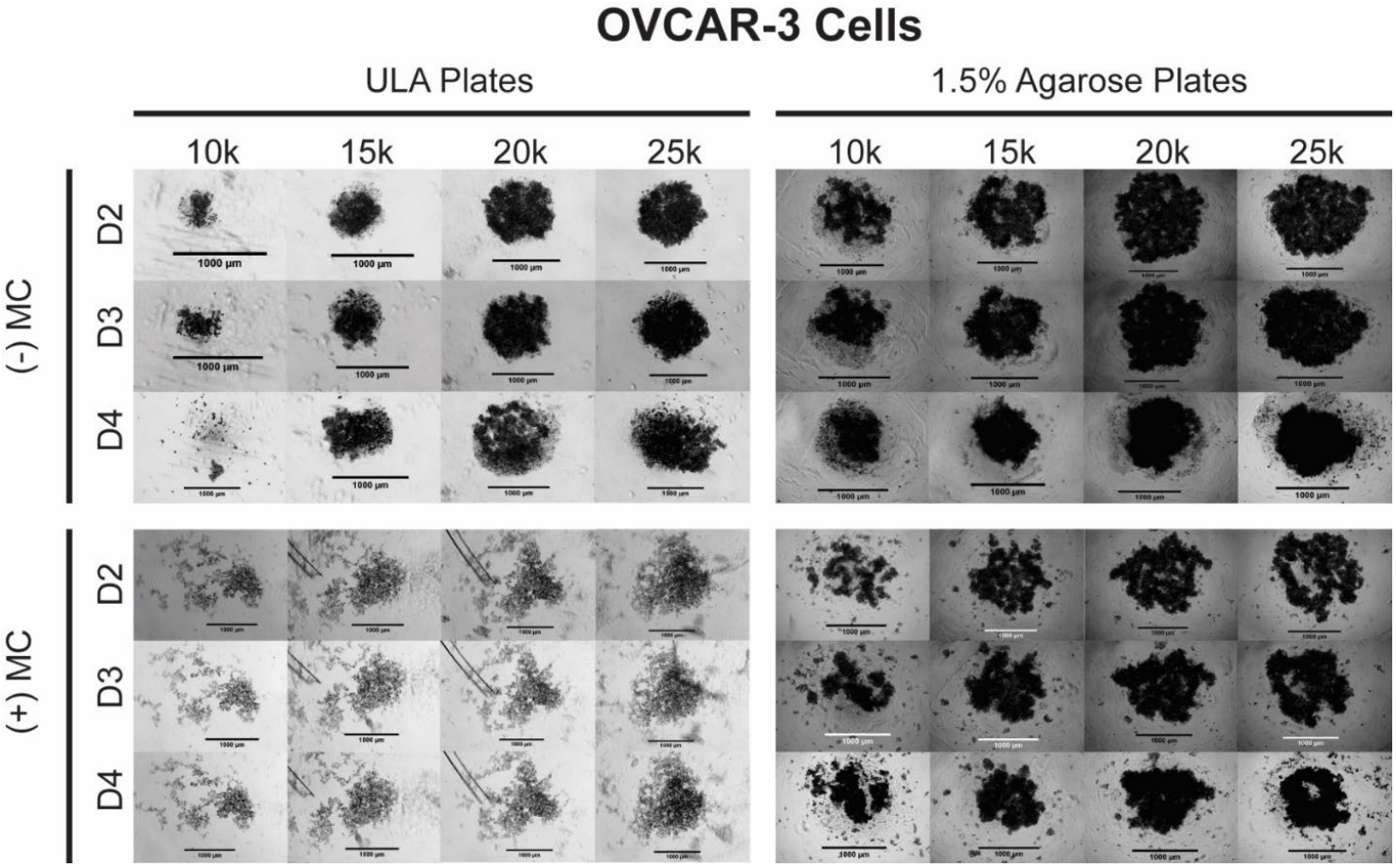

Figure 1: OVCAR-3 cells seeded with and without 0.5% methylcellulose in 1.5% agarose-coated and Ultra-Low Attachment 96-well plates over two, three, and four days at various seeding densities (10k corresponding to 10 x 10^3 cells seeded per well and so forth). All scale bars represent 1,000 µm; all images were taken at 4X objective.

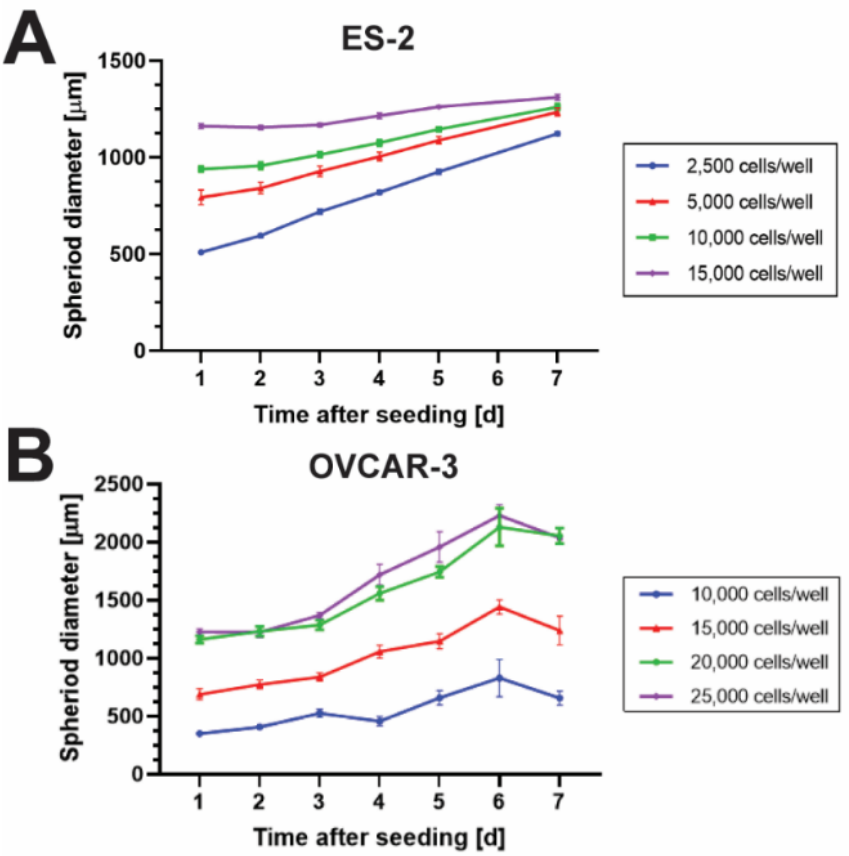

Figure 2: Spheroid diameters (A: ES-2 cells, B: OVCA-3 cells) over time in ULA plates without 0.5% MC. Diameters were measured via ImageJ at various time points and seeding densities (n = 3); error bars reflect mean ± SEM.

ES-2 cells: ES-2 cells were seeded in ULA and agarose-coated plates with and without 0.5% MC and imaged over the course of four days (Figure 3). We observed the formation of spheroids as soon as 24 hours after seeding on both culture surfaces, and this structure was maintained for up to seven days, however the tightest and roundest spheroids were formed when ES-2 cells were seeded using the ULA plates. Similar to the OVCAR-3 cells, we investigated the addition of MC in complete culture media and its effect on ES-2 spheroid compaction. In the agarose-coated plates, we observed that the addition of MC encouraged the formation of multiple, smaller spheroids of varying sizes, yet none

reached our desired 500-micron diameter threshold. The addition of MC to the ES-2 cells seeded in ULA plates completely discouraged spheroid formation at all. When measured over the course of seven days, the ES-2 spheroids grew steadily at consistent sizes within each seeding density, all of which resulted in spheroids greater than our 500-micron threshold 24 hours after seeding (Figure 3A). Given the improved structure and consistent formation of our ES-2 spheroids compared to our OVCAR-3 aggregates, we chose to complete the remainder of our study with only ES-2 cells cultured into spheroids via the ULA plate protocol.

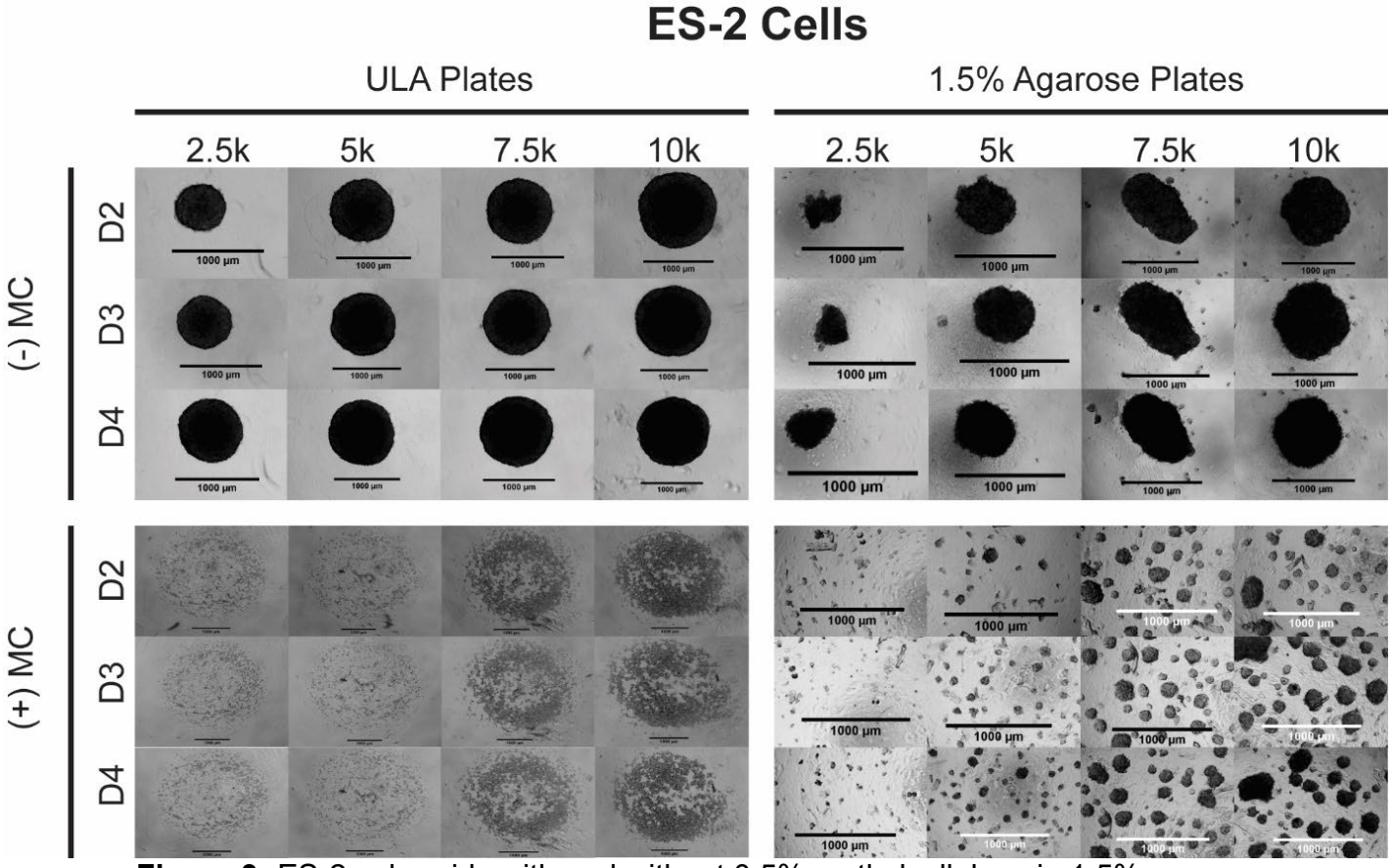

Figure 3: ES-2 spheroids with and without 0.5% methylcellulose in 1.5% agarose-coated and Ultra-Low Attachment 96-well plates over two, three, and four days at various seeding densities (5k corresponding to 5*10^3 cells seeded per well and so forth). All scale bars represent 1000 µm; all images taken at 4X objective.

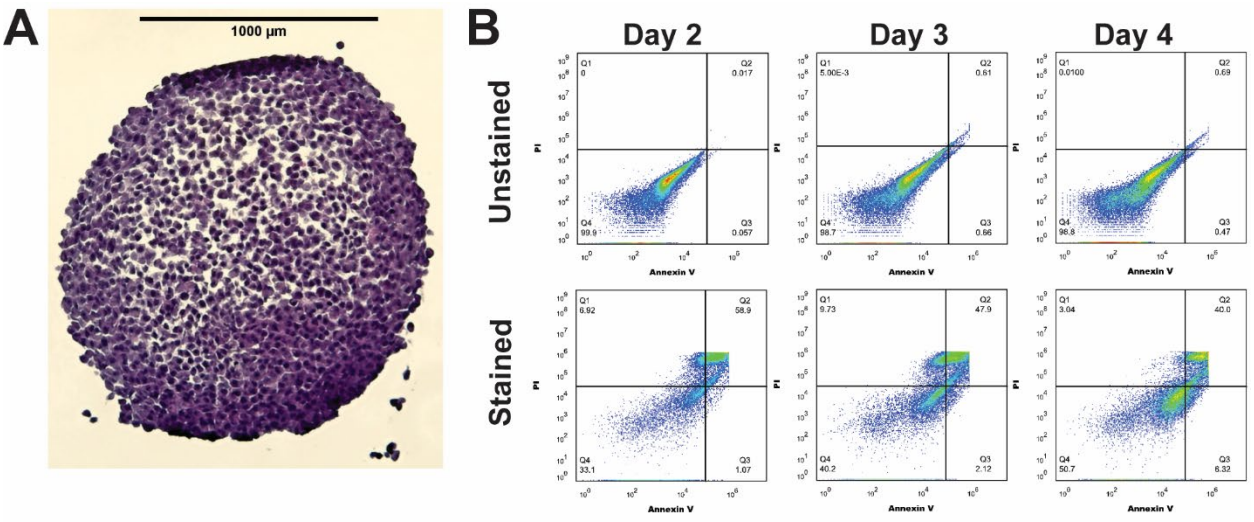

Figure 4: ES-2 Spheroid Section. 10,000 cells/well ES-2 spheroid grown in ULA plate and fixed on Day 3. Hematoxylin & Eosin-stained 5 µm-thick spheroid section taken from middle of spheroid. Purple stain represents cell nuclei; pink stain represents extracellular matrix. Image taken at 20X objective; scale bar represents 500 µm.

Spheroid development

The formation of spheroids that recapitulate clinical ovarian cancer behavior has been defined as those greater than 500 microns or greater in diameter, at which they should form three concentric cellular zones of proliferation, quiescence, and necrosis, respectively.[13] To confirm this development in our spheroids, we performed both qualitative and quantitative analyses of our ULA-cultured ES-2 spheroids. First, immunohistochemical sectioning and staining was performed on sections of 10,000 cells/well ES-2 spheroids three days after their seeding (Figure 3A). Tight, dense cellular nuclei and extracellular matrix was observed along the outer periphery of the spheroid, indicative of a proliferative region in which cells are communicating with each other. In contrast, the middle region of the spheroid displayed less extracellular matrix and sparse

nuclei, indicating that the cells at the interior of the spheroid may be necrotic or apoptotic. To quantify these cellular zones and the amount of the spheroid that they make up, we performed flow cytometric analyses on spheroids seeded at 10,000 cells/well, which were stained with Annexin V and Propidium Iodide (Figure 4B). Annexin V stains apoptotic cells by marking for the loss of plasma membrane asymmetry, and the latter is a nuclear and chromosome stain that selectively permeates in cells with a damaged membrane.[25,26]

Spheroid chemoresistance

The metabolic response of ES-2 cells when treated with Paclitaxel was compared between 2D and 3D culture methods. Figure 5 illustrates the ES-2 spheroids' inherent chemoresistance to PTX, shown by the maintenance of metabolic activity exhibited by 3D-cultured ES-2 cells compared to the significant decrease in metabolic activity exhibited by 2D cells when they are treated with varying micromolar concentrations of PTX over 48 hours. This PTX range was chosen because it encapsulates the half-maximal inhibitory concentration (IC_{50}) value we found for 2D-cultured ES-2 cells (0.3214 μM), however the IC_{50} value for 3D-cultured ES-2 cells treated with PTX was found to be 57.55 μM, further displaying the inherent chemoresistance that ES-2 cells develop when cultured in three dimensions that is not accurately reflected by two-dimensional cultures.

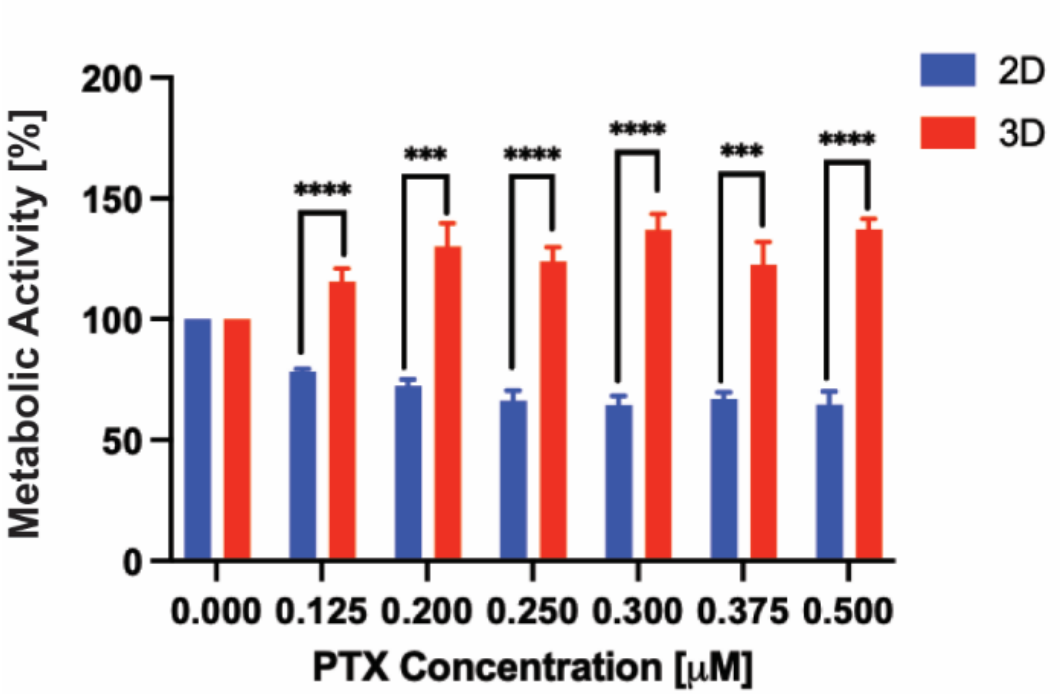

Figure 5: Metabolic activity of 2D and 3D (both 5,000 cells/well) ES-2 cells after treatment with varying concentrations of PTX for 48 hours (N = 3). Multiple t-test analyses where *** $p < 0.005$, **** $p < 0.001$, and $\alpha = 0.05$. 2D IC_{50} = 0.3214 μM, 3D IC_{50} = 57.55 μM.

Molecular profiles of 2D- and 3D-cultured ES-2 cells

To evaluate gene expression changes in the ES-2 spheroids compared to the 2D-cultured ES-2 cells, we performed western blotting and qPCR analyses, probing for two markers of chemoresistance: ABCB1 and CFLAR. ABCB1 is overexpressed in chemoresistant ovarian cancer, however when cultured in 3D, we saw decreased expression of this protein (Figure 6A). CFLAR is also overexpressed in ovarian cancer, and we saw an additional increase in its expression when ES-2 cells were cultured in 3D

versus 2D (Figure 6A), corroborated by a two-fold increase in its mRNA expression (Figure 6B).

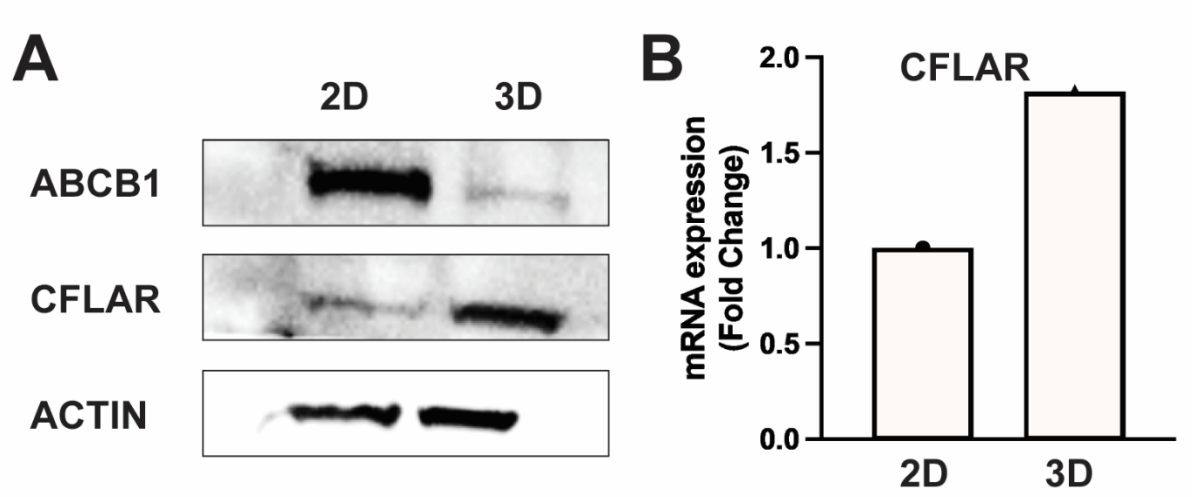

Figure 6: Basal expression of ABCB1 and CFLAR in ES-2 2D and 3D cultures. (A) Protein isolates collected after 4 days of growth for basal expression via western blotting. (B) RNA isolates collected after 4 days of growth for basal expression via qPCR (N=3).

Given our discovery that 2D and 3D cultures of ES-2 cells express different levels of known oncogenic proteins and genes, we sought to determine when these molecular differences occur. Through additional western blotting and qPCR, displayed in Figure 7, we determined that the aforementioned additional increased expression of CFLAR occurs after four days of spheroid growth. We also probed for the expression of STAT3, another oncogene with increased expression in ovarian cancers, and found that its expression decreased slightly after four days of spheroid growth.

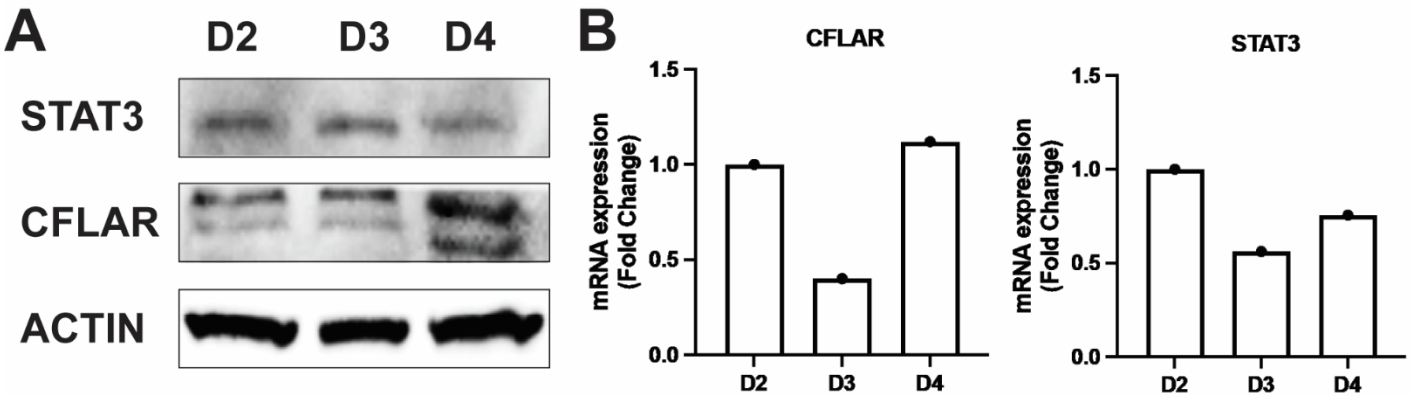

Figure 7: Basal expression of STAT3 and CFLAR in ES-2 spheroids over time. (A) Protein isolates from 20 ES-2 spheroids were collected for basal expression via western blotting. (B) RNA isolates from 5 spheroids were collected for basal expression via qPCR.

DISCUSSION

Ultra-low attachment well plates perform better than agarose-coated well plates when used for three-dimensional ovarian cancer cell culture.

Our first task in developing a uniform 3D-culturing method for *in vitro* ovarian cancer research was choosing between our two 96-well culture surfaces: 1.5% agarose-coated, flat-bottom plates or ultra-low attachment, round-bottom plates. We found that both of our cell lines formed more uniform, singular aggregates when cultured at multiple seeding densities in the ultra-low attachment plates. Additionally, our goal of optimizing an easily reproducible culturing method for ovarian cancer spheroids did not favor the creation of the agarose-coated well plates, as the agarose coatings were cumbersome and tedious to introduce to the well plates. It should be noted however, that we did not centrifuge our agarose-coated well plates after adding our cell suspensions, as we did with our ultra-low attachment plates, out of concern for comprising the integrity or position

of the agarose coating. Centrifugation may have encouraged better spheroid formation in the agarose-coated plates, however due to the comparatively very simple creation of spheroids that is capable with the ultra-low attachment plates, we chose to continue all of our experiments using only ULA plates.

ES-2 cells form compact spheroids, whereas OVCAR-3 cells form loose aggregates.

Our next task in creating our 3D ovarian cancer culture method was to investigate the spheroid formation capabilities of our two cells lines: ES-2 and OVCAR-3. Both of these cell lines are derived from epithelial ovarian cancer cell lines, a type of ovarian cancer that accounts for 90% of all diagnosed cases in the United States.[27] Over our entire course of seeding, the ES-2 spheroids formed more compact, dense spheroids that were more similar in size compared to the OVCAR-3 spheroids. Qualitatively, the ES-2 spheroids were very dense whereas the OVCAR-3 spheroids lacked tight boundaries and compaction and exhibited large holes, positing us to refer to them as aggregates rather than true spheroids.[45]

It should be noted that the OVCAR-3 aggregates and ES-2 spheroids were formed using seeding densities of different orders of magnitude. The seeding densities used for the OVCAR-3 spheroids were based on previous literature, however the OVCAR-3 cells are much smaller on average than ES-2 cells, based on observations during our cell culturing.[14] This is partly due to their different morphologies; OVCAR-3 cells are epithelial-like whereas ES-2 cells are spindle-like.[28] With this in mind, we chose to use smaller seeding densities for the ES-2 spheroids to avoid growing spheroids that were too large and exceeded the 96-well plate's working volume.

The amorphous aggregate structure that we observed with the OVCAR-3 cells has been noted in previous literature, and previous studies have demonstrated that different cell lines form spheroids of different morphologies due to their up- or downregulation of various cellular markers.[14,29] Specifically, OVCAR-3 cells are known to form loose aggregates compared to the compact spheroids formed by ES-2 cells, and previous studies have attributed this to an upregulation of E cadherin, an epithelial cell marker that plays a large role in cell-to-cell adhesion, in OVCAR-3 cells, as the accumulation of E cadherin on cell surfaces inhibits compact spheroid formation.[29,30,31,32]

Furthermore, in traditional 2D culture, OVCAR-3 cells are able to survive when both attached and in suspension, whereas ES-2 cells are adherence-dependent, based on the culture protocols from the American Type Culture Collection (ATCC). We hypothesize that because the OVCAR-3 cells are less dependent on attachment to and communication with their fellow cells, the aggregates formed by this cell line would tend to not compact as much based on a lack of necessity for survival. On the other hand, the ES-2 cells prefer to attach to one another, leading them to form tight, compact spheroids when unable to attach to a surface in order to survive. This trend is similar to what we see when we have used these two cells lines to create tumors in athymic mice for in vivo studies in the past; while the ES-2 cells formed relatively large tumors within days, the OVCAR-3 tumors did not mature until multiple weeks after subcutaneous and intraperitoneal injection.[48,49]

Because our lab employs the use of both ES-2 and OVCAR-3 cells in day-to-day experiments, we attempted to improve the formation of our OVCAR-3 aggregates into true spheroids. Based on this protocol's success in a study performed by Tofani et al, we

chose to add 0.5% W/V methylcellulose to the cell culture media of our spheroids.[14] Their results showed that the addition of methylcellulose in the media of OVCAR-3 spheroids increased the compactness and spherical nature of the spheroids, however the methylcellulose had the opposite effect on our spheroids; both the ES-2 and OVCAR-3 cells formed compact spheroids and aggregates without the addition of methylcellulose in both the ULA plates and agarose plates. The methylcellulose-treated cells lacked strong cell-to-cell adhesion and formed either large, amorphous clusters of cells or many very small aggregates rather than large, singular spheroids. Methylcellulose can be used as a thickening agent in water-based solvents, so it was proposed that its addition to the cell media would make the media solution slightly more viscous and prevent the ovarian cancer cells from migrating apart, thus encouraging tighter spheroid formation.[33]

These results were not observed in our study, possibly due to the thermosensitivity of methylcellulose.[34] An MC solution is liquid at room temperature, and as its temperature is increased past 37 degrees Celsius, the solution crosslinks and forms a hydrogel in a process known as thermogelation.[35] It is possible that the removal of the spheroid-containing plates from the 37 degree incubator for media changes and imaging was enough of a temperature change to affect the gelation of the media solution, causing stress to the cells and possibly causing a motile force that discouraged any spheroid/aggregate formation in either cell line. It is also possible that the methylcellulose underwent an adverse chemical reaction when exposed to the propriety coating that is used on the ULA plates we have employed. The surface is modified to be hydrophilic and have a neutral charge due to a covalently-bound hydrogel coating along the bottom of the plate which minimizes cell attachment, protein adsorption, and enzyme activation.[36,37]

ES-2 spheroids grow to uniform sizes, whereas OVCAR-3 aggregates are variable in size over time.

Lastly, when comparing our two possible ovarian cancer cell lines for spheroid formation, we measured our spheroids over the course of one week of growth. Literature states that ovarian cancer spheroids become replicative of *in vivo* tumor behavior once they reach a diameter of 500 microns or greater in diameter.[13] While both cell lines reached this threshold after only 24 hours, the plots of spheroid diameter over time in Figure 3 highlight that the ES-2 spheroids grew very steadily and had very small standard errors between the six spheroids measured. In contrast, the OVCAR-3 spheroids grew sporadically and had large error bars, meaning that the measured spheroids were not uniform in their size between technical replicates, despite their identical seeding. If we desire to use our spheroid models for repeated in vitro analyses, we favored the ES-2 cell line's growth curve, as it shows that from experiment to experiment, spheroids of the same seeding densities will grow to the same size, making them highly uniform and reproducible.

Overall, given the distinct morphological differences between the ES-2 spheroids and OVCAR-3 aggregates that we were able to form, our final formulation for successful ovarian cancer spheroid formation was to seed ES-2 cells in ultra-low attachment 96-well plates at a working volume of 100 microliters of cell culture media, without the addition of methylcellulose. We performed all subsequent experiments using this culture protocol.

3D ES-2 spheroids display three concentric cellular zones.

According to previous literature, one essential attribute of classifying a cellular aggregate as a spheroid is its development of three concentric cellular zones: a necrotic

core, a quiescent middle layer, and a proliferative periphery.[13] Through histological sectioning and staining, we have qualitatively observed the development of these cellular zones in the ES-2 spheroids cultured in the ULA plates. The hematoxylin and eosin stain of our spheroids illustrates that cellular nuclei along the outer edge of the spheroids are much closer together than those at the core of the spheroid. Additionally, the cells along the periphery are surrounded by a larger presence of extracellular matrix than the inner cells, likely because the former are actively communicating with each other and proliferating whereas the cells at the core are not because they have necrosed. The formation of extracellular matrix is likely an important factor in compact spheroid formation because it acts as a type of scaffold to hold the spheroid together, allowing the cells within to communicate with each other efficiently.[47]

To confirm our qualitative findings, we chose to evaluate the amount of live versus dead cells within our ES-2 spheroids over time using flow cytometry. By staining with Annexin-V and Propidium Iodide, which stain apoptotic cells by marking for the loss of plasma membrane asymmetry and stain dead cells by selectively permeating cells with compromised membranes, respectively. We found that as the spheroids grow, their population of live cells increases each day, which correlates to our positively-sloped growth curves and shows that our spheroids are proliferative over time. We also hypothesized that if our spheroids are growing over time, then the necrotic core should also increase in size, however we saw no trend in the number of necrotic cells in the spheroids over time. It is important to note that we did see populations of both live and dead cells within our spheroids, which is to be expected if the spheroids are appropriately developing concentric cellular zones that are activated by the metabolic and hypoxic

gradient that the cells experience due to the three-dimensional architecture of the spheroid structure. Additionally, cells that are marked as “dead” could also be cells that are live, however, through the process of obtaining single cell suspensions, membranes could undergo damage and disruption from mechanical separation.

3D ES-2 cultures exhibit increased chemoresistance in comparison to 2D cultures.

In comparison to 2D cultured cells, the 3D-cultured ES-2 cells displayed significantly increased metabolic activity after treatment with PTX. This indicates that the spheroid cultures exhibited significantly more chemoresistant to chemotherapeutics than the 2D cultures – a result replicative of *in vivo* tumor dose responses. The spheroid cultures can recapitulate *in vivo* tumor behavior *in vitro* when compared to traditional monolayer cell cultures. With increasing concentrations of PTX, the therapeutic response from the 3D spheroids remained stable which could be due various reasons including difficulty of drug penetration and increased expression of chemoresistant proteins. Therefore, we sought to analyze the molecular changes, if any, in protein and gene expression.

ES-2 cells express chemoresistance-associated proteins differently when cultured in two and three dimensions.

Knowing that the ES-2 spheroids are more chemoresistant than 2D cultures, we hypothesize that spheroids’ inherent chemoresistance has two origins. First, the structure of the spheroids allows them to have an inherent chemoresistance; cells within the quiescent middle layer and necrotic core of the spheroid are protected from chemotherapeutics because these treatments often cannot penetrate the multiple layers of cells required to reach all of the tumor’s cells.

Secondly, the increased cell-to-cell communication within the spheroids leads to the unique expression of proteins known be associated with chemoresistance, such as ABCB1, CFLAR, and STAT3, allowing them to exhibit an inherent chemoresistance that 2D-cultured ES-2 cells lack. In this study, we found that ABCB1, a drug efflux protein that is upregulated in ovarian cancer cells, is actually less abundant in 3D-cultured ES-2 cells than in 2D-cultures.[38] This is interesting because many researched ovarian cancer therapeutics currently target ABCB1 due to its relevance as a biomarker of poor ovarian cancer prognosis and multidrug resistance when overexpressed.[21,22] This gene target has shown success when studied in MDR ovarian cancer cell lines, however our results suggest that this may not be the best clinically translatable gene target.[39,40,46] Additionally studies would need to be conducted to examine the expression of ABCB1 in clinical tumors in comparison to 3D cultures.

We also investigated the expression of CFLAR, a Caspase-8 inhibitor that prevents apoptosis and is upregulated in ovarian cancer cells.[41] Our results show an exaggerated expression of CFLAR in 3D ovarian cancer cultures versus 2D cultures. This is a more novel gene target for ovarian cancer therapeutics; the expression of CFLAR is known to be a clinical prognostic factor of a poor disease outcome, and it has been found to be highly overexpressed in various cancers in comparison to healthy tissues.[42,23] Overexpression of CFLAR in our spheroids is expected based on our chemoresistance to PTX results because it would explain the spheroids' ability to evade apoptosis when treated with PTX.

The last objective of this study was to determine when these molecular differences within the spheroids arise. While our spheroids were classified as spheroids per literature

due to their 500-micron size after just 24 hours of growth, we wanted to determine when the optimal time to use the spheroids for experiments was, and we did this by determining at what day the spheroids underwent the aforementioned molecular changes in protein and gene expression. We determined that these molecular changes occurred on day 4 of the spheroids' growth, illustrated by an overexpression of CFLAR on this day. Interestingly, we saw no difference in the expression of STAT3, a transcription activator with proliferative, survival, and chemoresistive downstream effects, within the spheroids over time; however, this is evidence that the 3D-culture of ES-2 cells does not completely alter the cell's transcription and translation profile.[24] With these results, we chose to use our spheroids after four days of growth when using them for experiments *in vitro*.

CONCLUSIONS

The results of this study demonstrate that ES-2 cells can form uniform, compact spheroids of appropriate size for in vivo tumor recapitulation when cultured using a 3D culture protocol with ULA plates and standard cell culture media. However, OVCAR-3 cells are more likely to form large, loose aggregates that do not reflect the morphology of in vivo tumors. Additionally, the OVCAR-3 spheroid morphology was not improved when exposed to 0.5% methylcellulose, suggesting that this cell line is not ideal for spheroid formation nor the benefits of improved in vitro testing of anticancer therapies through the replacement of 2D-cultured cells with 3D cultures. The ES-2 spheroids displayed heightened chemoresistance to PTX compared to the 2D-cultured ES-2 cells and displayed concentric cellular zones of live and necrotic cells, confirming their classification as spheroids. The ES-2 spheroids also developed different molecular profiles in

comparison to 2D-cultured ES-2 cells, including an increased expression of chemoresistance-associated CFLAR, positing that the spheroids are inherently chemoresistant not only due to their architecture, but also due to unique cell-to-cell interactions.

The results obtained here indicate that spheroid cultures of ES-2 ovarian cancer cells may provide in vitro testing results that are accurately indicative of in vivo results in terms of metabolic activity, drug response, and uptake, in comparison to 2D-cultured ES-2 cells. This study also demonstrated the ability of ES-2 spheroids to reliably form spheroids of consistent size and shape, improving their reproducibility for both technical and biological replicates of *in vitro* assays.

In future, we would be interested to use our spheroid culture protocol with a healthy human-derived ovarian cell line to further investigate the molecular profiles of 3D-cultured ovarian cancer in comparison to healthy ovarian tissue. Tumor spheroids are also known to interact when placed within each other's vicinity, and this can affect their proliferation, survival, and protein expression.[43,44] While our spheroid-culturing protocol only allows for the creation of one spheroid per well plate at its onset, we could repeat the current study's investigation of inherent chemoresistance on spheroids that were transferred to the same well and allowed to grow together after their initial formation. Additionally, molecular profiles of intraperitoneal tumors grown *in vivo* and 3D-cultured can be tested for comparison.

ACKNOWLEDGEMENTS

This research was funded in-part by Materials Assembly and Design Excellence in South Carolina (MADE in SC) under National Science Foundation Award #OIA-1655740. Data presented in this publication was partially collected using SC BioCRAFT facilities supported by the National Institute of General Medical Sciences (NIGMS) of the National Institutes of Health under award number P30 GM131959. Any opinions, findings, conclusions, or recommendations expressed in the material are those of the author(s) and do not necessarily reflect the views of the National Science Foundation and National Institutes of Health. Support was also provided by Clemson College of Engineering, Computing, and Applied Sciences through their Undergraduate Opportunity research grant program, by the Clemson University Honors College, and by Clemson Creative Inquiry.

I would also like to acknowledge my advisor, Dr. Angela Alexander-Bryant. Thank you for adopting me into your lab and mentoring me into the scientist I am today. I always knew that I was interest in undergraduate research, but I never could have imagined the fruitful and amazing experience I've had, and I couldn't have done any of it without you or your support and guidance.

My greatest gratitude also goes to my graduate mentor, Kharimat Lora Alatise. Thank you for trusting me with a part of your doctoral work and allowing me to grow alongside you, both as a scientist and person, for the past two years. I will spend the entirety of my graduate career attempting to pay back all of the mentorship you've given me to my own undergraduate mentee, and I know it will be a breeze, because I've learned everything I know from the absolute best.

Lastly, a huge “thank you” to everyone in the Nanobiotechnology Lab, especially my other team members (Audrey Wessinger, Aaron Williams, Ruxi Xia) and my forever lab bestie, Carleigh Coffin.

REFERENCES

1. Doubeni, C. A., Doubeni, A. R., & Myers, A. E. (2016). Diagnosis and Management of Ovarian Cancer. *American family physician*, *93*(11), 937–944.
2. https://www.cancer.org/cancer/ovarian-cancer/about/key-statistics.html
3. C*ancer facts & figures 2023*. American Cancer Society. (2023). Retrieved from https://www.cancer.org/research/cancer-facts-statistics/all-cancer-facts-figures/2023-cancer-facts-figures.html
4. *Ovarian cancer stages and survival rate*. Cancer Treatment Centers of America. (2022, July 20). Retrieved from https://www.cancercenter.com/cancer-types/ovarian-cancer/stages
5. *Ovarian cancer facts*. Seattle Cancer Care Alliance. (n.d.). Retrieved from https://www.seattlecca.org/diseases/ovarian-cancer/facts
6. Centers for Disease Control and Prevention. (2022, August 31). *How is ovarian cancer treated?* Centers for Disease Control and Prevention. Retrieved from https://www.cdc.gov/cancer/ovarian/basic_info/treatment.htm
7. Li, S. S., Ma, J., & Wong, A. S. T. (2018). Chemoresistance in ovarian cancer: exploiting cancer stem cell metabolism. *Journal of gynecologic oncology*, *29*(2), e32. https://doi.org/10.3802/jgo.2018.29.e32
8. Fraser, M., Leung, B., Jahani-Asl, A. *et al.* Chemoresistance in human ovarian cancer: the role of apoptotic regulators. *Reprod Biol Endocrinol* **1**, 66 (2003). https://doi.org/10.1186/1477-7827-1-66
9. Ali, A. Y., Farrand, L., Kim, J. Y., Byun, S., Suh, J. Y., Lee, H. J., & Tsang, B. K. (2012). Molecular determinants of ovarian cancer chemoresistance: new insights into an old

conundrum. *Annals of the New York Academy of Sciences*, *1271*(1), 58–67. https://doi.org/10.1111/j.1749-6632.2012.06734.x

10. Yang, L., Xie, H. J., Li, Y. Y., Wang, X., Liu, X. X., & Mai, J. (2022). Molecular mechanisms of platinum-based chemotherapy resistance in ovarian cancer (Review). *Oncology reports*, *47*(4), 82. https://doi.org/10.3892/or.2022.8293
11. Alfarouk, K.O., Stock, CM., Taylor, S. *et al.* Resistance to cancer chemotherapy: failure in drug response from ADME to P-gp. *Cancer Cell Int* **15**, 71 (2015). https://doi.org/10.1186/s12935-015-0221-1
12. Nunes AS, Barros AS, Costa EC, Moreira AF, Correia IJ. 3D tumor spheroids as in vitro models to mimic in vivo human solid tumors resistance to therapeutic drugs. Biotechnol Bioeng. 2019 Jan;116(1):206-226. doi: 10.1002/bit.26845. Epub 2018 Oct 27. PMID: 30367820.
13. Zanoni, M., Cortesi, M., Zamagni, A. *et al.* Modeling neoplastic disease with spheroids and organoids. *J Hematol Oncol* **13,** 97 (2020). https://doi.org/10.1186/s13045-020-00931-0
14. Tofani, LB, Abriata, JP, Luiz, MT, Marchetti, JM, Swiech, K. Establishment and characterization of an in vitro 3D ovarian cancer model for drug screening assays. *Biotechnol Progress*. 2020; 36:e3034. https://doi.org/10.1002/btpr.3034
15. Meena, A. S., Sharma, A., Kumari, R., Mohammad, N., Singh, S. V., & Bhat, M. K. (2013). Inherent and acquired resistance to paclitaxel in hepatocellular carcinoma: molecular events involved. *PloS one*, *8*(4), e61524. https://doi.org/10.1371/journal.pone.0061524

16. Giannakeas, V., Sopik, V., & Narod, S. A. (2016). A model for ovarian cancer progression based on inherent resistance. Gynecologic oncology, 142(3), 484–489. https://doi.org/10.1016/j.ygyno.2016.06.014
17. Liang, R., Chen, X., Chen, L., Wan, F., Chen, K., Sun, Y., & Zhu, X. (2020). STAT3 signaling in ovarian cancer: a potential therapeutic target. *Journal of Cancer*, *11*(4), 837–848. https://doi.org/10.7150/jca.35011
18. McCorkle, J. R., Gorski, J. W., Liu, J., Riggs, M. B., McDowell, A. B., Lin, N., Wang, C., Ueland, F. R., & Kolesar, J. M. (2021). Lapatinib and poziotinib overcome ABCB1-mediated paclitaxel resistance in ovarian cancer. *PloS one*, *16*(8), e0254205. https://doi.org/10.1371/journal.pone.0254205
19. Mora-Molina, R., Stöhr, D., Rehm, M., & López-Rivas, A. (2022). cFLIP downregulation is an early event required for endoplasmic reticulum stress-induced apoptosis in tumor cells. *Cell death & disease*, *13*(2), 111. https://doi.org/10.1038/s41419-022-04574-6
20. Sun S, Cai J, Yang Q, Zhu Y, Zhao S, et al. (2016) Prognostic Value and Implication for Chemotherapy Treatment of ABCB1 in Epithelial Ovarian Cancer: A Meta-Analysis. PLOS ONE 11(11): e0166058. https://doi.org/10.1371/journal.pone.0166058
21. Wu Z-X, Yang Y, Wang J-Q, Zhou W-M, Chen J, Fu Y-G, Patel K, Chen Z-S and Zhang J-Y (2021) Elevated ABCB1 Expression Confers Acquired Resistance to Aurora Kinase Inhibitor GSK-1070916 in Cancer Cells. *Front. Pharmacol.* 11:615824. doi: 10.3389/fphar.2020.615824

22. Su, S., Sun, X., Zhang, Q., Zhang, Z., & Chen, J. (2019). CCL20 Promotes Ovarian Cancer Chemotherapy Resistance by Regulating ABCB1 Expression. *Cell structure and function*, *44*(1), 21–28. https://doi.org/10.1247/csf.18029
23. Fulda S. Targeting c-FLICE-like inhibitory protein (CFLAR) in cancer. Expert Opin Ther Targets. 2013 Feb;17(2):195-201. doi: 10.1517/14728222.2013.736499. Epub 2012 Dec 20. PMID: 23252466.
24. Liang, R., Chen, X., Chen, L., Wan, F., Chen, K., Sun, Y., & Zhu, X. (2020). STAT3 signaling in ovarian cancer: a potential therapeutic target. *Journal of Cancer*, *11*(4), 837–848. https://doi.org/10.7150/jca.35011
25. Wallberg, F., Tenev, T., & Meier, P. (2016). Analysis of Apoptosis and Necroptosis by Fluorescence-Activated Cell Sorting. *Cold Spring Harbor protocols*, *2016*(4), pdb.prot087387. https://doi.org/10.1101/pdb.prot087387
26. Kumar, R., Saneja, A., & Panda, A. K. (2021). An Annexin V-FITC-Propidium Iodide-Based Method for Detecting Apoptosis in a Non-Small Cell Lung Cancer Cell Line. *Methods in molecular biology (Clifton, N.J.)*, *2279*, 213–223. https://doi.org/10.1007/978-1-0716-1278-1_17
27. U.S. National Library of Medicine. (2021, October 8). *3 types of ovarian cancer, explained | NIH MedlinePlus Magazine*. MedlinePlus. Retrieved from https://magazine.medlineplus.gov/article/3-types-of-ovarian-cancer-explained
28. Beaufort CM, Helmijr JCA, Piskorz AM, Hoogstraat M, Ruigrok-Ritstier K, et al. (2014) Ovarian Cancer Cell Line Panel (OCCP): Clinical Importance of *In Vitro* Morphological Subtypes. PLOS ONE 9(9): e103988. https://doi.org/10.1371/journal.pone.0103988

29. Gunay G, Kirit HA, Kamatar A, Baghdasaryan O, Hamsici S, Acar H. The effects of size and shape of the ovarian cancer spheroids on the drug resistance and migration. Gynecol Oncol. 2020 Nov;159(2):563-572. doi: 10.1016/j.ygyno.2020.09.002. Epub 2020 Sep 18. PMID: 32958270.
30. Mao, M., Zheng, X., Jin, B., Zhang, F., Zhu, L., & Cui, L. (2017). Effects of CD44 and E-cadherin overexpression on the proliferation, adhesion and invasion of ovarian cancer cells. *Experimental and therapeutic medicine*, *14*(6), 5557–5563. https://doi.org/10.3892/etm.2017.5259
31. Powan, P., Luanpitpong, S., He, X., Rojanasakul, Y., & Chanvorachote, P. (2017). Detachment-induced E-cadherin expression promotes 3D tumor spheroid formation but inhibits tumor formation and metastasis of lung cancer cells. *American journal of physiology. Cell physiology*, *313*(5), C556–C566. https://doi.org/10.1152/ajpcell.00096.2017
32. Sodek, K. L., Ringuette, M. J., & Brown, T. J. (2009). Compact spheroid formation by ovarian cancer cells is associated with contractile behavior and an invasive phenotype. *International journal of cancer*, *124*(9), 2060–2070. https://doi.org/10.1002/ijc.24188
33. B. (n.d.). *Methylcellulose tips and troubleshooting*. Roger George Special Effects. Retrieved from https://rogergeorge.com/blogs/special-effects-guides/methylcellulose-tips-and-troubleshooting.
34. Niemczyk-Soczynska, B., Gradys, A., Kolbuk, D., Krzton-Maziopa, A., Rogujski, P., Stanaszek, L., Lukomska, B., & Sajkiewicz, P. (2022). A methylcellulose/agarose

hydrogel as an innovative scaffold for tissue engineering. *RSC advances*, *12*(41), 26882–26894. https://doi.org/10.1039/d2ra04841h

35. Rotbaum, Y., Parvari, G., Eichen, Y., Rittel, D. (2019) Mechanical reinforcement of methylcellulose hydrogels by rigid particle additives. Mechanics of Materials, 57-65, 132. 10.1016/j.mechmat.2019.02.013
36. corning Incorporated Life Sciences. (2014, July 22). Product Description: Costar ® 96-well Ultra Low Attachment, round bottom, with Low Evaporation lid. Retrieved from https://certs-ecatalog.corning.com/life-sciences/product-descriptions/7007.pdf
37. Corning Incorporated Life Sciences. (n.d.). *Corning® 96-well clear round bottom ultra-low attachment microplate, individually wrapped, with lid, sterile*. Corning. Retrieved from https://ecatalog.corning.com/life-sciences/b2c/US/en/Microplates/Assay-Microplates/96-Well-Microplates/Corning%C2%AE-96-well-Clear-Polystyrene-Microplates/p/7007
38. Christie, E. L., Pattnaik, S., Beach, J., Copeland, A., Rashoo, N., Fereday, S., Hendley, J., Alsop, K., Brady, S. L., Lamb, G., Pandey, A., deFazio, A., Thorne, H., Bild, A., & Bowtell, D. D. L. (2019). Multiple ABCB1 transcriptional fusions in drug resistant high-grade serous ovarian and breast cancer. *Nature communications*, *10*(1), 1295. https://doi.org/10.1038/s41467-019-09312-9
39. Wu, D. D., Li, X. S., Meng, X. N., Yan, J., & Zong, Z. H. (2016). MicroRNA-873 mediates multidrug resistance in ovarian cancer cells by targeting ABCB1. *Tumour biology : the journal of the International Society for Oncodevelopmental Biology and Medicine*, *37*(8), 10499–10506. https://doi.org/10.1007/s13277-016-4944-y

40. Tian, S., Zhang, M., Chen, X., Liu, Y., & Lou, G. (2016). MicroRNA-595 sensitizes ovarian cancer cells to cisplatin by targeting ABCB1. *Oncotarget*, *7*(52), 87091–87099. https://doi.org/10.18632/oncotarget.13526
41. Kostova, I., Mandal, R., Becker, S., & Strebhardt, K. (2021). The role of caspase-8 in the tumor microenvironment of ovarian cancer. *Cancer metastasis reviews*, *40*(1), 303–318. https://doi.org/10.1007/s10555-020-09935-1
42. Bagnoli, M., Ambrogi, F., Pilotti, S., Alberti, P., Ditto, A., Barbareschi, M., Galligioni, E., Biganzoli, E., Canevari, S., & Mezzanzanica, D. (2009). c-FLIPL expression defines two ovarian cancer patient subsets and is a prognostic factor of adverse outcome, *Endocrine-Related Cancer*, *16*(2), 443-453. Retrieved Apr 22, 2023, from https://doi.org/10.1677/ERC-08-0218
43. Białkowska, K., Komorowski, P., Bryszewska, M., & Miłowska, K. (2020). Spheroids as a Type of Three-Dimensional Cell Cultures-Examples of Methods of Preparation and the Most Important Application. *International journal of molecular sciences*, *21*(17), 6225. https://doi.org/10.3390/ijms21176225
44. Gunti, S., Hoke, A. T. K., Vu, K. P., & London, N. R., Jr (2021). Organoid and Spheroid Tumor Models: Techniques and Applications. *Cancers*, *13*(4), 874. https://doi.org/10.3390/cancers13040874
45. Han, S.J., Kwon, S. & Kim, K.S. Challenges of applying multicellular tumor spheroids in preclinical phase. *Cancer Cell Int* **21**, 152 (2021). https://doi.org/10.1186/s12935-021-01853-8

46. Alatise, K. L., Gardner, S., & Alexander-Bryant, A. (2022). Mechanisms of Drug Resistance in Ovarian Cancer and Associated Gene Targets. *Cancers*, *14*(24), 6246. https://doi.org/10.3390/cancers14246246
47. Gonçalves IG, Garcia-Aznar JM (2021) Extracellular matrix density regulates the formation of tumour spheroids through cell migration. PLoS Comput Biol 17(2): e1008764. https://doi.org/10.1371/journal.pcbi.1008764
48. Zhang, X. Y., Li, Y. F., Ma, H., & Gao, Y. H. (2020). Regulation of MYB mediated cisplatin resistance of ovarian cancer cells involves miR-21-wnt signaling axis. *Scientific reports*, *10*(1), 6893. https://doi.org/10.1038/s41598-020-63396-8
49. Samec, T., Alatise, K. L., Boulos, J., Gilmore, S., Hazelton, A., Coffin, C., & Alexander-Bryant, A. (2022). Fusogenic peptide delivery of bioactive siRNAs targeting CSNK2A1 for treatment of ovarian cancer. *Molecular therapy. Nucleic acids*, *30*, 95–111. https://doi.org/10.1016/j.omtn.2022.09.012
50. Nik Nabil, W. N., Xi, Z., Song, Z., Jin, L., Zhang, X. D., Zhou, H., De Souza, P., Dong, Q., & Xu, H. (2021). Towards a Framework for Better Understanding of Quiescent Cancer Cells. *Cells*, *10*(3), 562. https://doi.org/10.3390/cells10030562
51. Cardano, M., Tribioli, C., & Prosperi, E. (2020). Targeting Proliferating Cell Nuclear Antigen (PCNA) as an Effective Strategy to Inhibit Tumor Cell Proliferation. Current cancer drug targets, 20(4), 240–252. https://doi.org/10.2174/1568009620666200115162814
52. Alimbetov, D., Askarova, S., Umbayev, B., Davis, T., & Kipling, D. (2018). Pharmacological Targeting of Cell Cycle, Apoptotic and Cell Adhesion Signaling

Pathways Implicated in Chemoresistance of Cancer Cells. *International journal of molecular sciences*, *19*(6), 1690. https://doi.org/10.3390/ijms19061690